[Au18(dppm)6Cl4]4+: Phosphine-Protected Gold Nanocluster with Rich Charge States

Dalton Trans

Dalton Transactions

Dynamic Article Links ▶

ARTICLE

[Au18(dppm)6Cl4]4+: Phosphine-Protected Gold Nanocluster with Rich Charge States

Shan-Shan Zhang,[a,⊥] **Ravithree D. Senanayake,**[b,⊥] **Quan-Qin Zhao,**[a] **Hai-Feng Su,**[c,*] **Christine M. Aikens,**[*,b] **Xing-Po Wang,**[*,a,] **Chen-Ho Tung,**[a] **Di Sun**[*,a,c] **and Lan-Sun Zheng**[c]

A diphosphine-protected 18-gold-atom nanocluster was isolated via a facile reduction of a Au^I precursor by $NaBH_4$. Its composition was identified as {[Au18(dppm)6Cl4]·C6H6·3Cl·PF6} (**SD/Au18**, **SD** = SunDi; dppm = Bis-(diphenylphosphino)methane) by X-ray single crystal structural analysis. This nanocluster possesses a prolate shape and is built from a Au_{10} kernel (bi-octahedral Au_6 units sharing one
10 edge) fused with two Au_7 caps *via* sharing six gold atoms. The identity of the Au_{18} cluster is further demonstrated by ESI-MS. The number of valence electrons of [Au18(dppm)6Cl4]4+ is 10 (n^* = 18–4–4), which does not match with known magic numbers according to the spherical jellium model, and elongated models must be considered. The special stability of the Au_{18} cluster likely arises from geometrical factors in the metallic core. Two charge states are reported for this system. This work not only presents the structure elucidation of a diphosphine-protected Au_{18} nanocluster, but also provides important insight into the growth pattern of gold nanoclusters and the charge
15 states they can achieve.

Introduction

Since the first X-ray structure determination of the decahedral Au_{102} cluster by the Kornberg group in 2007,[1] the field of atomically precise gold nanoclusters started to bloom due to their
20 role as bridges between small organo-gold molecules and plasmonic gold nanoparticles. Owing to their size-dependent properties,[2] uncovering the atomically precise structures of gold nanoclusters is of supreme significance for understanding their compositions, stability, metal atom packing fashion, metal-ligand
25 interfacial bonding as well as physicochemical properties.[3] Although the growth of high-quality single crystals of gold nanoclusters is a huge challenge and has been haunting chemists for a long time, several phosphine,[4] thiolate,[5] and alkynyl-protected[6] gold nanoclusters with X-ray structure characterizations
30 have been reported. Gold-thiolate nanoclusters have experienced explosive development from 2007 until now,[7] however the

phosphine-protected gold nanoclusters that started much earlier developed relatively slowly.[8] Although several groups including Konishi, Hutchison, Hudgens, and Wang have carried out
35 extensive studies on gold-phosphine clusters, to date only limited gold-phosphine clusters have been reported such as the first X-ray structure determined Au_{11},[9] diphosphine-protected icosahedral Au_{13},[10] Au_{14},[11] Au_{18},[12] chiral Au_{20},[13] Au_{22}[14] and Au_{39}.[15] The largest gold-phosphine cluster hitherto known is a 55-gold-atom
40 nanocluster protected by PPh_3 but the crystal structure and chemical composition has been elusive.[16] Compared to the multitude of gold-thiolate nanoclusters, why have so few gold-phosphine clusters been isolated? Is it possible to isolate a series of gold-phosphine nanoclusters as cousins of gold-thiolate
45 nanoclusters? To answer these questions many more experimental studies are needed, especially that obtain vivid single crystal structures.

aKey Laboratory of Colloid and Interface Chemistry, Ministry of Education, School of Chemistry and Chemical Engineering, and State Key Laboratory of Crystal Materials, Shandong University, Jinan, 250100, People's Republic of China.
E-mail: dsun@sdu.edu.cn. xpw6@sdu.edu.cn. Fax: +86-531-88364218.
bDepartment of Chemistry, Kansas State University, Manhattan, Kansas 66506, USA. Email: cmaikens@ksu.edu
cState Key Laboratory for Physical Chemistry of Solid Surfaces and Department of Chemistry, College of Chemistry and Chemical Engineering, Xiamen University, Xiamen 361005, People's Republic of China. Emai: hfsu@xmu.edu.cn
⊥These authors contributed equally to this work.
†Electronic Supplementary Information (ESI) available. Detailed synthesis procedure, tables, crystal data in CIF files, IR, EDX and UV-Vis for **SD/Au18**. CCDC 1572857. For ESI and crystallographic data in CIF

Fig 1. Positive electrospray ionization mass spectrometry (ESI-MS) of the
50 Au_{18} nanocluster dissolved in methanol. Inset: The measured (black trace) and simulated (red trace) isotopic patterns.

Results and discussion

X-ray Structures of {[Au$_{18}$(dppm)$_6$Cl$_4$]·C$_6$H$_6$·3Cl·PF$_6$} (SD/Au18).

With these considerations in mind, we revisited the dppm-
[5] protected gold nanocluster system, and herein report the synthesis and total structure determination of a 18-gold-atom nanocluster in the formula of {[Au$_{18}$(dppm)$_6$Cl$_4$]·C$_6$H$_6$·3Cl·PF$_6$} (**SD/Au18**). This gold nanocluster has the following features: (a) it contains an Au$_{10}$ kernel built by two *fcc*-type Au$_6$
[10] octahedra sharing one edge; (b) it belongs to an unusual 10 free electrons family of gold nanoclusters; (c) it can exist in multiple charge states.

Scheme 1. Upper: Synthetic Routes for [Au$_{18}$(dppm)$_6$Cl$_4$]$^{4+}$. Bottom left: Schematic Structure of Octadecanuclear Gold Nanocluster. Bottom right:
[15] Numbering of Unique Nine Gold Atoms in **SD/Au18** and the Other Nine are Generated by Crystallographic Inversion Center Highlighted by a Black Dot.

$$[Au_2(dppm)_2Cl_2] \xrightarrow[^nBu_4NPF_6]{THF/MeOH \quad NaBH_4} [Au_{18}(dppm)_6Cl_4]^{4+}$$
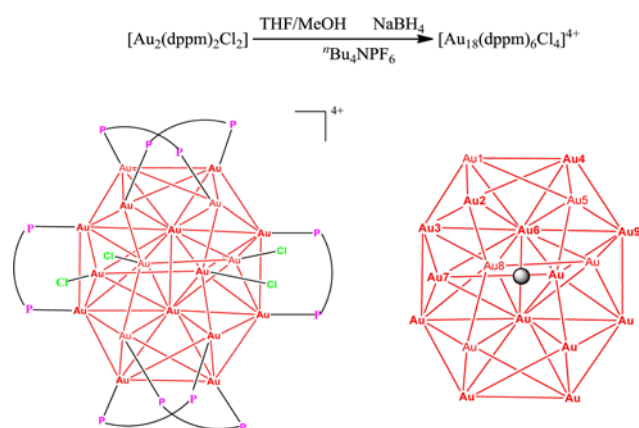
SD/Au18 was synthesized by direct reduction of
[20] [Au$_2$(dppm)$_2$Cl$_2$][17] with NaBH$_4$ in the presence of ^{n}BuNPF$_6$ in a mixture of CH$_3$OH and THF. Crystallization and single crystal growth of **SD/Au18** were performed by liquid/liquid diffusion of benzene to a concentrated solution of **SD/Au18** in CH$_2$Cl$_2$ for one week. The sample of **SD/Au18** was collected as
[25] black crystals for other characterization such as electrospray ionization mass spectrometry (ESI-MS), infrared spectroscopy (IR), UV-Vis and so on. Details of the synthesis are shown in the Electronic Supplementary Information (†ESI). The chemical composition of **SD/Au18** was verified by electrospray
[30] ionization mass spectrometry (ESI-MS), which shows only a predominant peak at *m/z* = 2996.4816 with a characteristic isotopic peak separation of *m/z* = 0.5, corresponding to [Au$_{18}$(dppm)$_6$Cl$_4$]$^{2+}$ (calcd. *m/z* = 2996.4966). The correctness of assignment is also confirmed by the well-matched observed
[35] and experimental isotope patterns (Figure 1). The bulk of the sample collected from the test tubes was confirmed to be the same to the single crystals by comparing the measured X-ray powder diffraction pattern with that simulated from single-crystal data (Figure S1). Infrared spectrum (Figure S2) band at
[40] 834 cm^{-1} indicates the existence of PF$_6^-$ in **SD/Au18**. The mass spectrometry data demonstrates that although **SD/Au18** was isolated in the +4 charge state in the crystal structure, it can also achieve a +2 charge state. A similar [Au$_{18}$(dppm)$_6$Br$_4$]$^{2+}$ system was previously crystallized,[12] suggesting that this

[45] particle can access multiple charge states, and may undergo reversible oxidation and reduction. Previously, several thiolate-stabilized nanoclusters such as Au$_{25}$[5d] and Au$_{144}$[18] have been found to undergo reversible oxidation and reduction, but this phenomenon has not been achieved before in phosphine-
[50] stabilized nanoparticles.
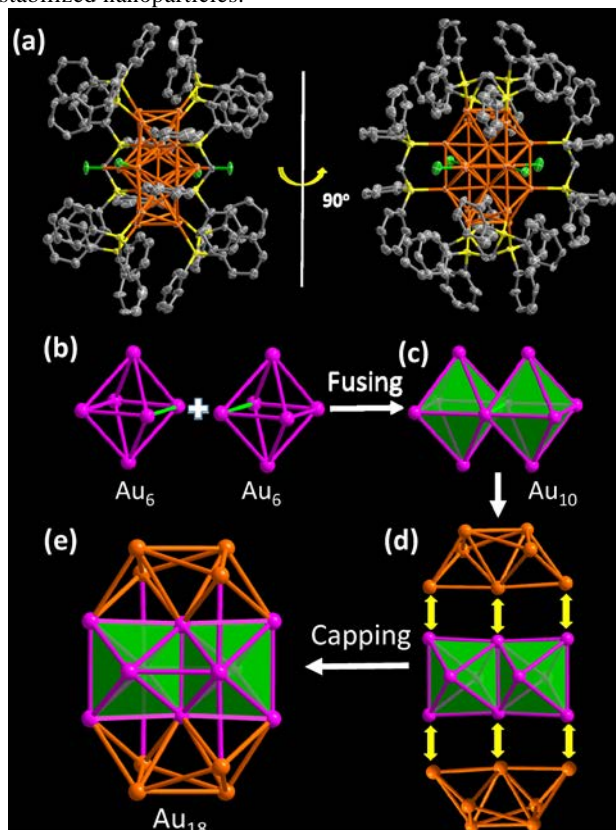
Fig 2. (a) The X-ray crystal structure of cationic [Au$_{18}$(dppm)$_6$Cl$_4$]$^{4+}$ viewed along two orthogonal directions. Thermal contours are drawn at the 50% probability level. (b) A pair of octahedral Au$_6$ units fused by edge-sharing
[55] (green edge) to form an Au$_{10}$ kernel shown by polyhedral mode (c). (d) Two Au$_{12}$ caps fused on the two longer edges of Au$_{10}$ kernel. (e) The metallic core of Au$_{18}$. Color labels: golden/purple, Au; yellow, P; gray, C. H atoms and lattice Cl$^-$ and PF$_6^-$ ions are omitted.

The total structure of **SD/Au18** was determined by single crystal
[60] diffraction analysis (Table S1). It crystallizes in triclinic space group *P*-1 and the nanocluster sits on the crystallographic inversion center, thus the asymmetric unit contains only a half of Au$_{18}$ nanocluster. As shown in Figure 2a, the overall structure of **SD/Au18** is a prolate configuration composed of 18 gold atoms,
[65] six bidentate dppm ligands, and four terminal chlorides. The counteranions for [Au$_{18}$(dppm)$_6$Cl$_4$]$^{4+}$ are three Cl$^-$ and one PF$_6^-$. The average atomic ratio of P and Cl measured from three different regions of one crystal is 13.0 : 7.2 which is well matched with the expected ratio of 13 : 7 (Figure S3). Thermogravimetric analysis
[70] (TGA) reveals that **SD/Au18** is stable until 120 °C. A weight loss of 4.0 % was found from 120 to 290 °C, corresponding to the losing of guest counter anions including three Cl$^-$ and one PF$_6^-$ (calcd. 3.9 %). Further heating to 366 °C, the weight loss of 40.3% is due to the decomposition of six dppm ligands and four terminal
[75] chlorides (calcd. 40.7 %) from **SD/Au18** (Figure S4). The basic kernel in the Au$_{18}$ nanocluster is the *fcc*-type Au$_6$ octahedron

(Figure 2b), which can be deemed as a perfect fragment cut out from face-centered-cubic (*fcc*) bulk gold. Two octahedral Au_6 units share one edge (Au6-Au6^i) to form a Au_{10} kernel (Figure 2c) similar to $[Au_{18}(dppm)_6Br_4]^{2+}$. The Au-Au separations in the Au_6 octahedron fall in the range of 2.7230(2)-2.9843(15) Å (average 2.863 Å), which is slightly shorter than the bulk gold Au-Au distance (2.88 Å). The bi-octahedral Au_{10} kernel is further fused together with two Au_7 caps by sharing two longer edges (Au3-Au6-Au9) of the Au_{10} kernel (Figure 2d). Each Au_7 cap is composed of four face-shared tetrahedra and the Au-Au distances within the cap are in the range 2.7431(16)-2.8999(16) Å (average 2.803 Å), which is shorter than those in the Au_{10} kernel. The prolate Au_{18} nanocluster has two poles and a waist. Two shorter edges (Au3-Au9) of the Au_{10} kernel as well as its four vertexes (Au7 × 2 and Ag8 × 2) are in the waist region. Four Cl^- ions coordinate to the four vertex sites with Au-Cl bond lengths of 2.3440(7) Å and 2.3730(7) Å. Two shorter edges of the Au_{10} kernel are clamped by two dppm ligands. Each pole (Au1, Au2, Au18 and Au5) is coordinated to two bidentate dppm ligands. In total, six dppm and four terminal chloride ligands wrap the surface of the Au_{18} nanocluster to stabilize it. The dimension of the Au_{18} core is 7.37 × 4.59 Å without considering the outside ligands (Figure 2e).
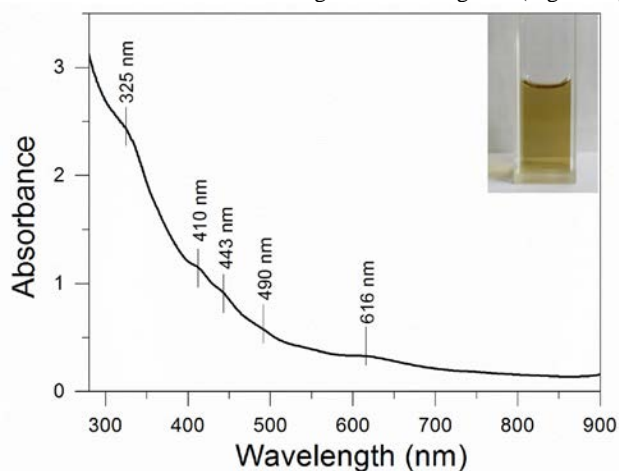
Fig 3. UV−vis absorption spectrum of **SD/Au18** in CH_3OH.

Optical Properties and Time-Dependent DFT (TDDFT) Calculations of SD/Au18.

SD/Au18 has very good solubility in methanol. As revealed by time-dependent UV-Vis spectra, it did not show obvious changes after its solution was stored under ambient conditions for one week (Figure S5), indicating its high stability in solution. The optical absorption spectrum of **SD/Au18** was recorded in methanol solution, and is shown in Figure 3. The absorption spectrum of **SD/Au18** showed a predominant peak at 325 nm along with three weak shoulder peaks at 410, 443, 490 nm, and another weak peak at 616 nm.

Interestingly, the $[Au_{18}(dppm)_6Cl_4]^{4+}$ cluster nominally possesses 10 free valence electrons, that is 18(Au atoms) – 0 (ligands) − 1 × 4(chlorides) – 4 = 10e, which neither agrees with magic numbers for the case of spherical shell closure,[19] nor the 2D electron-counting requirement.[20] Due to its prolate geometry, the electronic stability of the 10e Au_{18} cluster may be rationalized using the Clemenger-Nilsson ellipsoidal shell model,[21] which has

been used to explain the 14e $Au_{38}(SR)_{24}$ and 16e $[Au_{20}(PP_3)_4]^{4+}$ (PP_3 = tris(2-(diphenylphosphino)ethyl)phosphine) systems.[4b, 22] For Au_{18}, the disorder parameter (δ) is calculated to be 0.47 from the equation $δ = 2(R_x-R_z)/(R_x+R_z)$,[23] where R_x and R_z are the lengths of maximum and minimum diameters for metal core. This δ value matches well with that of 0.45 predicted from the Clemenger-Nilsson model for an alkali metal cluster with ten valence electrons.

The $[Au_{18}(dppm)_6Cl_4]^{q+}$ system is of significant interest because it appears to be able to access two charge states. As described above, **SD/Au18** has a +4 charge state in the crystal structure and +2 in mass spectrometry, whereas the $[Au_{18}(dppm)_6Br_4]^{2+}$ cluster[12] possesses a +2 charge state in its crystal structure. Density functional theory (DFT) calculations are used in the current work to analyze the electronic structure of the $[Au_{18}(dppm)_6Cl_4]^{q+}$ (q = 4, 2) nanocluster. Two structures are considered in the theoretical calculations: the crystal structure and a model structure in which the phenyl groups in the dppm ligands were replaced by hydrogen atoms to simplify the structure. Additional computational details are provided in the Electronic Supplementary Information.

The DFT orbital energy diagram and frontier Kohn-Sham orbitals of the $[Au_{18}(dppm)_6Cl_4]^{2+}$ cluster are shown in Figure 4. The HOMO has $Π_1$-like character arising from the 6sp atomic orbitals of gold atoms in the core mixed with significant contributions from the 5d orbitals of gold; the cylindrical $Π_1$-like character is due to the ellipsoidal gold core of this cluster and the lobes of the orbital are oriented toward the four chloride ligands. The HOMO-1 and HOMO-2 mainly have $Σ_3$-like character mixed with 5d character; these orbitals are nearly degenerate with a 0.04 eV splitting. The HOMO-3 is an orbital with $Π_1$-like character in which the lobes of the $Π_1$ orbital are oriented towards two chloride and two phosphine groups. The $Π_1$ orbitals are not doubly degenerate because the two short axes of the nanocluster are not identical. Orbitals directly below HOMO-3 have significant contributions from chloride 3p atomic orbitals, with the gold 5d band below. For $[Au_{18}(dppm)_6Cl_4]^{2+}$, the singly-degenerate LUMO and LUMO+1 have $Π_2$ and $Π_3$ character, respectively. The LUMOs immediately above the LUMO+1 primarily arise from π* orbitals on the phenyl groups, although some orbitals including LUMO+7 also have significant contributions from the Au 6sp orbitals.

The electronic structure of the model $[Au_{18}(PH_2CH_2PH_2)_6Cl_4]^{2+}$ system is very similar to that of the full nanocluster, with the exception that the LUMO+2 and higher orbitals do not have phenyl π* contributions. The HOMO-LUMO gap of the model system is 1.364 eV compared to 1.476 eV for the full $[Au_{18}(dppm)_6Cl_4]^{2+}$ system. The absorption spectra for both the full and model nanocluster systems are shown in Figure 5.

There are several significant excitations in the absorption spectra of the +2 systems that have relatively high oscillator strengths, weights and transition dipole moments. The $[Au_{18}(PH_2CH_2PH_2)_6Cl_4]^{2+}$ exhibits an excitation at 1.47 eV which is primarily the HOMO → LUMO transition. The excitation around 2.22 eV has a relatively high oscillator strength value (0.1477) where HOMO-2 → LUMO+2 is the main transition that contributes to the excitation. The $[Au_{18}(dppm)_6Cl_4]^{2+}$ spectra also

displays a prominent excitation around 1.54 eV which is predominantly the HOMO → LUMO transition. An excitation around 2.07 eV has a high oscillator strength similar to the $[Au_{18}(PH_2CH_2PH_2)_6Cl_4]^{2+}$ spectrum. Unlike in the model system, the excitation is mainly composed of two transitions: HOMO →

LUMO+14 and HOMO-2 → LUMO+7. The LUMO+7 in this system has the same Au 6sp character as the LUMO+2 in the model system. Other significant excitations for both systems are shown in Tables S3 and S4.
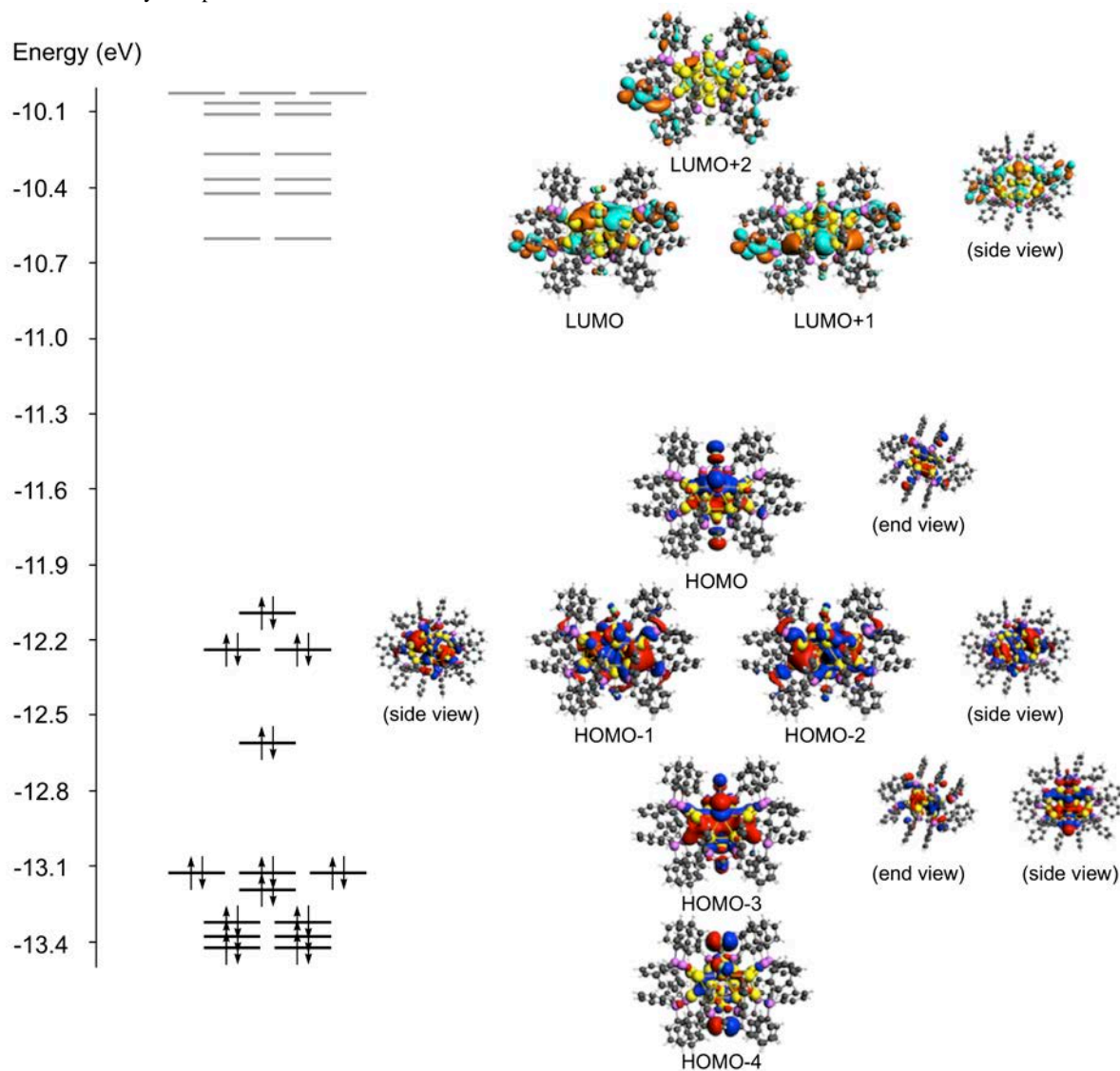
Fig 4. Kohn-Sham orbitals and orbital energy diagram for $[Au_{18}(dppm)_6Cl_4]^{2+}$ at the LB94/DZ level of theory.

Although a small gap (0.14 eV) is present between the HOMO and HOMO-1 for the full $[Au_{18}(dppm)_6Cl_4]^{2+}$ nanocluster, DFT calculations on the $[Au_{18}(dppm)_6Cl_4]^{4+}$ system did not converge due to its resulting small HOMO-LUMO gap (additional details are provided in the ESI). However, calculations on the model $[Au_{18}(PH_2CH_2PH_2)_6Cl_4]^{4+}$ cluster converged, and the HOMO-LUMO gap of this system was found to be only 0.026 eV. The DFT results suggest that the most favorable charge state for the $Au_{18}(dppm)_6Cl_4^{q+}$ cluster is +2; observation and isolation of the +4 charge state in **SD/Au18** suggests that this system could undergo reversible oxidation and reduction.

The $[Au_{18}(PH_2CH_2PH_2)_6Cl_4]^{4+}$ spectrum (Figure 5c) with the smaller HOMO-LUMO gap agrees well with the experimental absorption spectra for **SD/Au18** and with that reported for the

$[Au_{18}(dppm)_6Br_4]^{2+}$ by Zhu and coworkers.[12] The absorption spectrum gives significant peaks around 640, 502, 469 and 325 nm. Overall, the calculated spectra of the +4 and +2 charge states appear similar with minor structure apparent on a broad background.

In the calculated spectrum, the peak around 640 nm is composed of three main excitations that have relatively high oscillator strengths. The main transitions involved are HOMO→ LUMO+2, HOMO-1→ LUMO+2 and HOMO-18→ LUMO. Similar to the HOMO-1 and HOMO-2 of $[Au_{18}(PH_2CH_2PH_2)_6Cl_4]^{2+}$, the HOMO and HOMO-1 of $[Au_{18}(PH_2CH_2PH_2)_6Cl_4]^{4+}$ mainly have Σ_3-like character mixed with d character due to the rod-shaped elongated gold core of this cluster. The HOMO-18 is a delocalized Σ_3-like orbital. The LUMO+2 has Π_3 character while the LUMO is a Π_1-

type orbital. The peak around 502 nm, which is the strongest in terms of the oscillator strength, is composed of transitions to LUMO+4 from HOMO-1 and HOMO. This can be assigned to a strong transition polarized along the long axis of the nanocluster with $\Sigma_3 \rightarrow \Sigma_4$ character. The 469 nm peak, which comes from two main excited states, has contributions from the HOMO-5$\rightarrow$LUMO+1, HOMO-2$\rightarrow$LUMO+3 and HOMO-6$\rightarrow$LUMO+1 transitions, where the HOMO-5 and HOMO-6 are a mixture of Au 5d atomic orbitals and 3p orbitals from Cl. The LUMO+1 has Π_2 character and the LUMO+3 has Δ_1-like character.
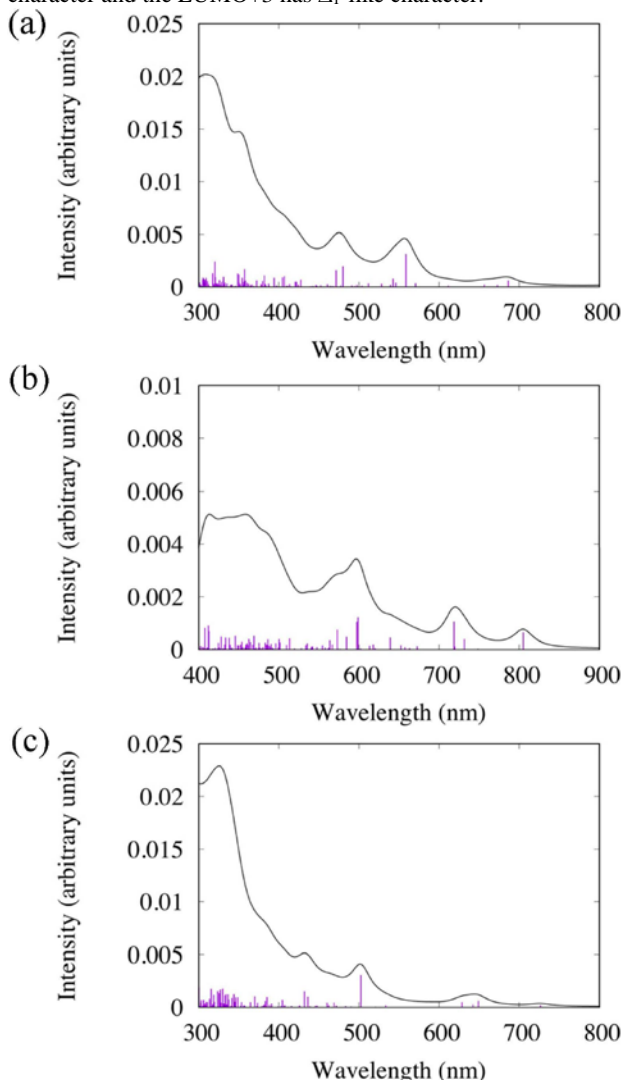
Fig 5. Theoretical absorption spectra of (a) $[Au_{18}(PH_2CH_2PH_2)_6Cl_4]^{2+}$, (b) $[Au_{18}(dppm)_6Cl_4]^{2+}$ and (c) $[Au_{18}(PH_2CH_2PH_2)_6Cl_4]^{4+}$ calculated at the LB94/DZ level of theory.

Conclusions

In conclusion, we isolated and characterized a dppm-protected Au_{18} nanocluster that contains an Au_{10} kernel built from two octahedral Au_6 units *via* edge sharing. The Au_6 octahedron can be seen as the smallest piece in *fcc* bulk gold**.** The nanocluster can access two charge states, and could be the first phosphine-stabilized nanocluster to undergo reversible oxidation and reduction. It is expected that our work may motivate more studies on phosphine-protected gold nanoclusters.

References

1. P. D. Jadzinsky, G. Calero, C. J. Ackerson, D. A. Bushnell, R. D. Kornberg, *Science*, 2007, **318**, 430-433.
2. (a) G. Schmid, *Chem. Soc. Rev.*, 2008, **37**, 1909-1930; (b) R. C. Jin, *Nanoscale*, 2010, **2**, 343-362; (c) J. F. Parker, C. A. Fields-Zinna, R. W. Murray, *Acc. Chem. Res.*, 2010, **43**, 1289-1296; (d) Y. Lu, W. Chen, *Chem. Soc. Rev.*, 2012, **41**, 3594-3623; (e) H. F. Qian, M. Z. Zhu, Z. K. Wu, R. C. Jin, *Acc. Chem. Res.*, 2012, **45**, 1470-1479; (f) P. Maity, S. Xie, M. Yamauchi, T. Tsukuda, *Nanoscale*, 2012, **4**, 4027-4037; (g) G. Li, R. C. Jin, *Acc. Chem. Res.*, 2013, **46**, 1749-1758; (h) S. Yamazoe, K. Koyasu, T. Tsukuda, *Acc. Chem. Res.*, 2014, **47**, 816-824; (i) S. Knoppe, T. Bürgi, *Acc. Chem. Res.*, 2014, **47**, 1318-1326.
3. R. C. Jin, C. J. Zeng, M. Zhou, Y. X. Chen, *Chem. Rev.*, 2016, **116**, 10346-10413.
4. (a) L. Y. Yao, V. W.-W. Yam, *J. Am. Chem. Soc.,* 2016, **138**, 15736-15742; (b) X.-K. Wan, S.-F. Yuan, Z.-W. Lin, Q.-M. Wang, *Angew. Chem., Int. Ed.*, 2014, **53**, 2923-2926; (c) N. Kobayashi, Y. Kamei, Y. Shichibu, K. Konishi, *J. Am. Chem. Soc.*, 2013, **135**, 16078-16081; (d) Y. Shichibu, K. Konishi, *Small*, 2010, **6**, 1216-1220; (e) Y. Kamei, Y. Shichibu, K. Konishi, *Angew. Chem.*, *Int. Ed.*, 2011, **50**, 7442-7445; (f) Q.-F. Zhang, P. G. Williard, L.-S. Wang, *Small*, 2016, **12**, 2518-2525.
5. (a) C. J. Zeng, Y. X. Chen, K. Kirschbaum, K. J. Lambright, R. C. Jin, *Science*, 2016, **354**, 1580-1584; (b) R. C. Jin, *Nanoscale*, 2015, **7**, 1549-1565; (c) R. C. Jin, *Nanoscale*, 2010, **2**, 343-362; (d) M. Z. Zhu, C. M. Aikens, F. J. Hollander, G. C. Schatz, R. C. Jin, *J. Am. Chem. Soc.*, 2008, **130**, 5883-5885; (e) D. Crasto, G. Barcaro, M. Stener, L. Sementa, A. Fortunelli, A. Dass, *J. Am. Chem. Soc.*, 2014, **136**, 14933-14940; (f) M. W. Heaven, A. Dass, P. S. White, K. M. Holt, R. W. Murray, *J. Am. Chem. Soc.*, 2008, **130**, 3754-3755; (g) C. J. Zeng, Y. X. Chen, K. Kirschbaum, K. Appavoo, M. Y. Sfeir, R. C. Jin, *Sci. Adv.*, 2015, **1**, e1500045; (h) W. Kurashige, Y. Niihori, S. Sharma, Y. Negishi, *Coord. Chem. Rev.*, 2016, **320-321**, 238-250; (i) H. F. Qian, M. Z. Zhu, Z. K. Wu, R. C. Jin, *Acc. Chem. Res.*, 2012, **45**, 1470-1479; (j) S. Chen, S. X. Wang, J. Zhong, Y. B. Song, J. Zhang, H. T. Sheng, Y. Pei, M. Z. Zhu, *Angew. Chem., Int. Ed*., 2015, **54**, 3145-3149; (k) D. Crasto, S. Malola, G. Brosofsky, A. Dass, H. Häkkinen, *J. Am. Chem. Soc.*, 2014, **136**, 5000-5005; (l) Y. X. Chen, C. J. Zeng, C. Liu, K. Kirschbaum, C. Gayathri, R. R. Gil, N. L. Rosi, R. C. Jin, *J. Am. Chem. Soc.*, 2015, **137**, 10076-10079; (m) H. F. Qian, W. T. Eckenhoff, Y. Zhu, T. Pintauer, R. C. Jin, *J. Am. Chem. Soc.*, 2010, **132**, 8280-8281.
6. (a) X.-K. Wan, Q. Tang, S.-F. Yuan, D.-e Jiang, Q.-M. Wang, *J. Am. Chem. Soc.*, 2015, **137**, 652-655; (b) X. K. Wan, S. F. Yuan, Q. Tang, D.-e Jiang, Q. M. Wang, *Angew. Chem., Int. Ed.*, 2015, **54**, 5977-5980; (c) X. K. Wan, W. W. Xu, S. F. Yuan, Y. Gao, X. C. Zeng, Q. M. Wang, *Angew. Chem., Int. Ed*., 2015, **54**, 9683-9686.
7. C. J. Zeng, Y. X. Chen, K. Kirschbaum, K. J. Lambright, R. C. Jin, *Science*, 2016, **354**, 1580-1584.
8. K. Konishi, In *Gold Clusters, Colloids and Nanoparticles I*; D. M. P. Mingos, Ed.; Structure and Bonding; Springer International Publishing: Berlin, 2014, **161**, 49-86.

9.   M. McPartlin, R. Mason, L. Malatesta, *J. Chem. Soc., Chem. Commun.*, 1969, **7**, 334-334.

10.   Y. Shichibu, K. Suzuki, K. Konishi, *Nanoscale*, 2012, **4**, 4125-4129.

11.   B. S. Gutrath, I. M. Oppel, O. Presly, I. Beljakov, V. Meded, W. Wenzel, U. Simon, *Angew. Chem., Int. Ed.*, 2013, **52**, 3529-3532.

12.   S. Jin, W. J. Du, S. X. Wang, X. Kang, M. Chen, D. Q. Hu, S. Chen, X. J. Zou, G. D. Sun, M. Z. Zhu, *Inorg. Chem.*, 2017, **56**, 11151-11159.

13.   (a) X.-K. Wan, Z.-W. Lin, Q.-M. Wang, *J. Am. Chem. Soc.*, 2012, **134**, 14750-14752; (b) J. Chen, Q.-F. Zhang, P. G. Williard, L.-S. Wang, *Inorg. Chem.*, 2014, **53**, 3932-3934.

14.   J. Chen, Q.-F. Zhang, T. A. Bonaccorso, P. G. Williard, L.-S. Wang, *J. Am. Chem. Soc.*, 2014, **136**, 92-95.

15.   B. K. Teo, X. B. Shi, H. Zhang, *J. Am. Chem. Soc.*, 1992, **114**, 2743-2745.

16.   G. Schmid, R. Pfeil, R. Boese, F. Bandermann, S. Meyer, G. H. M. Cali, W. A. Vandervelden, *Chem. Ber.*, 1981, **114**, 634-3642.

17.   I. J. B. Lin, J. M. Hwang, D.-F. Feng, M. C. Cheng, Y. Wang, *Inorg. Chem.*, 1994, **33**, 3469-3472.

18.   H. F. Qian, R. C. Jin, *Chem. Mater.* 2011, **23**, 2209-2217.

19.   H. Hakkinen, *Chem. Soc. Rev.*, 2008, **37**, 1847-1859.

20.   M. Walter, P. Frondelius, K. Honkala, H. Hakkinen, *Phys. Rev. Lett.*, 2007, **99**, 096102.

21.   (a) K. Clemenger, *Phys. Rev. B.*, 1985, **32**, 1359-1362; (b) S. G. K. Nisson, *Dan. Vidensk. Selsk. Mat. Fys. Medd.* 1955, **29**, 16.

22.   Y. Pei, Y. Gao, X. C. Zeng, *J. Am. Chem. Soc.*, 2008, **130**, 7830-7832.

23.   Y. Pei, Y. Gao, N. Shao, X. C. Zeng, *J. Am. Chem. Soc.*, 2009, **131**, 13619-13621.

Graphical Abstract